Facile synthesis of Co-N_4-doped mesoporous carbon for oxygen reduction reaction

Hong Zhao [a], Caina Su[b], K.N. Hui [c,*], K.S. Hui [a,*]

[a] *School of Mathematics, University of East Anglia, Norwich, NR4 7TJ, United Kingdom*

[b] *School of Chemical and Environmental Engineering, Institute of Applied Chemistry, Shanxi Datong University, Datong 037009, China*

[c] *Institute of Applied Physics and Materials Engineering, University of Macau, Avenida da Universidade, Taipa, Macau*

[*]Corresponding author:

Email addresses: bizhui@umac.mo (K.N. Hui)

Tel: +853-8822-4426; Fax: +853-8822-2426

E-mail: k.hui@uea.ac.uk (K.S. Hui)

Tel: +44 (0)1603 592582; Fax: +44 (0)1603 593345

Abstract

The oxygen reduction reaction (ORR) is a critical factor in fuel cells that has attracted significant research attention. Non-precious metal catalysts have improved the ORR activity considerably, but they still exhibit poorer ORR performance than commercial Pt-based catalysts. In this study, Co-N_4-doped mesoporous carbon (Co-N_4-MC) was prepared for the ORR using cobalt-azides as the Co-N_4-containing precursor, and ordered mesoporous silica SBA-15 as a template for achieving mesoporous structures. The Co-N_4-MC electrode exhibited remarkable ORR activity in an alkaline medium (a half-wave potential of -0.15V vs. MMO, only ~ 19 mV deviation from the commercial Pt/C catalyst), high selectivity (electron-transfer number ~ 4) and excellent electrochemical stability (~ 8 mV negative shift of the half-wave potential after 1000 cycles). The good performance of the Co-N_4-MC electrode was attributed to the synergetic effects of N_4, C and Co. In particular, the existence of graphitic pores in the Co-N_4-MC catalyst facilitated the diffusion of O_2 to the catalytic active sites, which benefited the progression of the ORR on the Co-N_4-MC catalyst.

Keywords: Co-N_4-doped mesoporous carbon; Oxygen reduction reaction; Graphitic pores

1. Introduction

The activity of the oxygen reduction reaction (ORR) is a critical factor in fuel cells and other electrochemical technologies (1). The low reaction rate of the ORR can be overcome using expensive nano-sized Pt catalysts in fuel cells (2, 3). In addition to the scarcity and high-cost, the long-term operation of fuel cells may lead to dissolution and agglomeration of the noble metal particles, which will degraded the performance of the electrocatalysts (4-6). The search for efficient, durable and inexpensive non-precious metal catalysts has become one of the most active and competitive endeavors in the study of energy conversion (7-12). Recently, these non-precious metal and nitrogen doped carbon catalysts prepared from transition metal macrocyclic compounds, such as Co-N_4-C and Fe-N_4-C, are considered the best alternative ORR electrocatalysts (13-16). On the other hand, the unavoidable agglomeration of carbon materials hinders the diffusion of electrolyte ions to the catalytic active sites, thereby reducing the catalytic performance. Mesoporous carbon (MC)-based catalysts can effectively allow the reactants to access the catalytic active sites efficiently, leading to improved mass transport in electrochemical reactions. (17-19). Therefore, Co-N_4-MC could be a good candidate for the ORR, combining the good catalytic activity of the Co-N_4-C catalyst with the excellent mass-transfer performance of MC (20, 21). Despite this, there are few reports on the activity of the ORR over Co-N_4-MC (22, 23), which may be due to the expensive Co sources, such as Vitamin B12 (24, 25) and cobalt tetramethylphenylporphyrin (CoTMPP) (9, 26, 27). Large amounts of CoTMPP are required to produce Co-N_4-C catalysts, making it an expensive preparation process.

Although some simple inorganic salt containing Co are used as the Co source (28), however, Co nanoparticles formed in the catalyst composite instead of Co–N_4 clusters (29). According to density functional theory analysis (30), only Co–N_4 clusters near the graphite material can promote the four-electron pathway of the ORR. Therefore, it is still a challenge to develop a low-cost and effective Co source to produce stable Co-N_4 doped carbon materials as the ORR catalysts.

This paper reports a novel, effective and low-cost method to produce Co-N_4-MC via a high temperature graphitizing process. The novelties in this work, compared to the earlier works (31), are (i) the synthesis of organo-cobalt compounds as the Co-N_4-containing precursor in a low-cost manner, and (ii) use of commercial SBA-15 (pore size of 20 nm) as the template to produce Co-N_4-MC with a mesoporous structure (pore size of 4.2 nm) to enhance the accessibility of O_2 and the electrolyte to the catalytic activity sites. SBA-15 has been successfully large-scale produced in industries, which would benefit to the industrial production of Co-N_4-MC catalyst which achieved a stable and high performance comparable to the commercial Pt/C catalyst in ORR, as supported by the current study.

2. Experimental Section

2.1. Preparation of the Co-N_4 complex

The Co-N_4 complex was synthesized via four reactions, as shown in step 1 of Figure 1. The first three reactions were based on a previous study (32), which is a typical method to synthesize the N_4 complex. To the best of the authors' knowledge, this is the

first report of the preparation of a Co-N_4 complex using the proposed method. Compound a (20g) was heated with K_2CO_3 (10% wt.) and 1-iodopropane (7% wt.) in anhydrous CH_3CN under reflux in a N_2 atmosphere. Compound b was obtained from the reaction mixture by extraction with CH_2Cl_2, and subsequent precipitation with methanol. Compound d was obtained by the purification of compound c (20g) with N-bromosuccinimide and azobis in CCl_4. Subsequently, compounds b and d were heated under reflux in anhydrous CH_3CN (200ml) in the presence of Cs_2CO_3 (5% wt.) under nitrogen to synthesize compound e. Finally, the Co-N_4 complex was prepared by mixing Co^{2+} ions and compound e at a molar ratio of 1:1.

2.2. Preparation of Co-N_4-MC

Ordered mesoporous silica, SBA-15 (Sigma-Aldrich), was used as a template to produce the mesoporous carbon structures [19]. The SBA-15 template (1 g) was impregnated with a solution of 50 mg of anhydrous oxalic acid in 200 mL ethanol (pure grade) for 20 min (33). In step 2, the oxalic acid-treated SBA-15 was then impregnated with 2 g of the Co-N_4 complex for 45 min at room temperature. In step 3, the resulting composite was then subjected to a series of thermal treatments including 60 °C for 30 min, 100 °C for 5 h and 200 °C for 5 h. Stepwise heating was used to evaporate and decompose the organic solvent. At the final thermal treatment, the resulting sample was transferred to a tube furnace for carbonization at 900 °C for 3 h under a N_2 atmosphere at a heating rate of 10 °C/min. In step 4, the SBA-15 template was removed using 15% hydrofluoric acid (200 mL). Co-N_4-MC was obtained after rinsing the sample three times with 50 mL butanol (pure grade). For comparison, the graphitic N_4-C and the

template-free Co-N_4-C were also prepared by heating the compound e and the target compound, respectively, at the same heating conditions. The commercial carbon-supported Pt catalyst from Sigma-Aldrich (labeled as Pt/C, with 10 wt.% of Pt metal loading) was used for comparison (34).

2.3. Sample characterizations

The morphology of the samples was analyzed by scanning electron microscopy / energy dispersive X-ray spectroscopy (SEM/EDX, JEOL JMS820). Transmission electron microscopy (TEM, JEOL Model JEM-2000F) images were obtained using a high-resolution system with a LaB_6 filament at 200 kV. The sample powder was dispersed in ethanol by sonication for 3 h, and drops of the suspension were deposited on a copper grid with a holey carbon film. The sample was air-dried and kept in a microscope vacuum for 15 min before the tests. X-ray diffraction (XRD, Philips, model PW 1830) of the prepared samples were obtained using Cu-Kα radiation (λ = 0.1542 nm) at 40 kV and 30 mA. The scanning speed was 0.25° min^{-1} with a 0.02° step. The BET (Brunauer, Emmett and Teller) surface areas of the samples were investigated using a N_2 adsorption–desorption apparatus (Micromeritics ASAP 2020M) at liquid nitrogen temperature (-196 °C). The surface elemental composition of the samples was determined by X-ray photoelectron spectroscopy (XPS, VG Scientifics ESCALAB250). Raman spectroscopy was performed using a micro-Raman spectrometer (Renishaw, InVia). A glassy carbon electrode (GCE) with an area of 0.125 cm^2 was used as the working electrode. Pt foil was employed as the counter electrode, and Hg/HgO/KOH (1.0 M) (MMO, 0.098 V versus SHE) was used as the reference electrode. The working

electrode was modified with the catalyst layer by placing the catalysts on the GCE. The catalyst ink was prepared by dispersing 10 mg of the each sample ultrasonically in 1.9 mL of ethanol, to which 0.1 mL of a 5 wt.% Nafion solution was added. The dispersion was ultrasonicated for 30 min to obtain a homogeneous solution. Approximately 10 μL of the dispersion was pipetted out on the top of the GCE and dried in air.

3. Results and Discussion

3.1. Characterizations of Co-N_4-MC

Formation of the Co-N_4 complex was first confirmed by UV-vis spectra, which shows the UV-vis spectra of the N_4 complex before and after complexing with Co^{2+} ions. The N_4 compound had an absorption band at 286 nm, which was assigned to the absorption of the phenyl and 2,2-dipyridyl moieties. The addition of Co^{2+} ions to the N_4 compound caused a shift of the ligand absorption band from 286 nm to 308 nm. These results indicated the formation of the Co-N_4 complex. Interestingly, the formation process of Co-N_4-MC can be traced by TEM. As shown in Figure S2a, the skeletons and the pore channels of SBA-15 were observed, whereas only the skeletons of SBA-15 were observed after the pore channels of SBA-15 had been filled with the Co-N_4 complex (Figure S2b). After removing the SBA-15 template with hydrofluoric acid, the skeletons and pore channels of SBA-15 became invisible (Figure S2c). Figure 2a-c shows TEM images of the Co-N_4-MC sample at different magnifications. EDX confirmed the presence of C, N and Co in the Co-N_4-MC sample (Figure 2b). Figure 2c showed that the Co and N doped pyrolytic carbon consisted of graphene-like sheets. On the other

hand, no Co NPs were observed, even at high magnification. This is because when Co-macrocyclic compounds were used as the Co source, Co-N_4 nanoclusters were generally formed [21] instead of Co NPs [23]. Figure 2d-f show SEM images with mapping, clearly indicating the density of CKα1, NKα1 and CoKα1. As shown in Figure 3a, the Co-N_4-MC sample exhibited the typical shape for a mesoporous material (20, 35). The mesopore radius distribution was centered at approximately 4.2 nm (Figure 3b). In Figure 3c, the Raman spectra revealed the characteristic peaks of graphitic carbon at 1350 cm^{-1} (D-band), 1580 cm^{-1} (G-band) and 2750 cm^{-1} (2D-band). The narrow D- and G-bands as well as an intense 2D-band indicated that the Co-N_4-MC sample had high crystallinity.

As shown in Figure 4a, the atomic percentage of N, C and Co in the Co-N_4-MC sample were 4.36 %, 94.67 % and 0.97 %, respectively (impurities, such as trace amounts of O, Si and F were not detected). Figure 4b-d show the high-resolution N1s, C1s and Co2p spectra. The C1s peak (Figure 4b) was shifted to a higher binding energy (284.9 eV), which was attributed to the incorporation of nitrogen (36, 37). In Figure 4c, the N1s peak was fitted to peaks of pyridinic-N (398.2 eV), pyrrolic-N (4001 eV), and graphitic-N (400.7 eV). Among them, pyridinic-N (up to 42 at.% of the total amount of N atoms) was found to critically affect the ORR performance (38-40). In addition, the peaks for $Co2p_{3/2}$ and $Co2p_{1/2}$ (Figure 4d) were observed in the Co-N_4-MC sample, confirming the existence of Co (0) atoms.

3.2. Electrochemical activity of Co-N_4-MC electrode for ORR

To evaluate the ORR performance of the Co-N_4-MC electrode and other electrodes,

the polarization curves for the ORR of the electrodes were recorded in a 0.1 M KOH solution saturated with pure oxygen. Figure 5a shows the linear sweep voltammetry curves of the electrodes. Typically, the positive onset potential and half-wave potential, and high current density are good metrics for a good ORR catalyst. These results indicated that the onset potential (–0.02 V vs. MMO) and half-wave potential (–0.15 vs. MMO) of the Co-N_4-MC electrode are similar to those of the Pt/C electrode. The onset potential of the Co-N_4-MC electrode is much higher than those of the N_4-C electrode (-0.15 V vs. MMO) and the Co-N_4-C electrode (-0.017 V vs. MMO) and the half-wave potential is higher than those of the N_4-C electrode (-0.25 V vs. MMO) and the Co-N_4-C electrode (-0.20 V vs. MMO) as well. The limited current (5.4 mA cm^{-2}) of the Co-N_4-MC electrode approached that of the Pt/C electrode (5.5 mA cm^{-2}), and was higher than those of the N_4-C electrode (3.8 mA cm^{-2}) and the Co-N_4-C (4.5 mA cm^{-2}) electrode (15). For the Co-N_4-MC electrode, the Co atoms could facilitate the incorporation of active N species into the carbon matrix with strong Lewis basicity, which enhances the electron-donor properties of the N-doped carbon and weakens the O-O bond via bonding with the oxygen and nitrogen and/or the adjacent carbon atom (36). The N atoms, particularly pyridinic-N, make an important contribution to the ORR performance (38-40). In addition, the existence of the graphitic pores in the Co-N_4-MC electrode sample could facilitate the diffusion of O_2 to the Co-N_4 active sites, and benefit the progression of the ORR on the Co-N_4-MC electrode (41, 42). However, the N_4-C electrode, without the Co catalysts, showed a different ORR mechanism from the Co-N_4-MC electrode (43). For the Co-N_4-C electrode, without the mesoporous carbon

structure, although it has similar onset potential, the limit current is much lower than that of the Co-N_4-MC electrode, which could be due to the poor mass transfer performance (44). The results suggest that the high performance of the Co-N_4-MC electrode is due to the synergetic effects of N, Co and MC structure in the Co-N_4-MC sample.

To confirm the 4e-ORR reaction path, a series of rotating disk voltammograms of the ORR by the Co-N_4-MC electrode at different rotation rates in a 0.1 M KOH saturated with oxygen were tested (Figure 5b). The RDE data was analyzed using the Kouteckye–Levich equation (45):

$$\frac{1}{J} = \frac{1}{J_K} + \frac{1}{J_L} = \frac{1}{J_K} + \frac{1}{B\omega^{1/2}} \quad (1)$$

$$B = 0.62nFC_{O_2} D_{O_2}^{\frac{2}{3}} v^{-\frac{1}{6}} \quad (2)$$

$$J_K = nFkC_{O_2} \quad (3)$$

where J is the measured current density, J_K and J_L are the kinetic and diffusion limiting current densities, respectively, ω is the electrode rotation rate, n is the overall number of electron transfer, F is the Faraday constant (96,485 C mol^{-1}), C_o is the bulk concentration of O_2 dissolved in the electrolyte (1.2×10^{-6} mol cm^{-3}), D_o is the O_2 diffusion coefficient (1.9×10^{-5} cm^2 s^{-1}), and v is the kinematic viscosity of the electrolyte (v = 0.01 cm^2 s^{-1}) (46). Based on the ring and disk currents, the calculated number (n) of electrons transfer is approximately 3.85 for the Co-N_4-MC electrode (Figure 5c), which was confirmed by the measured n value (Figure 5d) using the rotating ring-disk electrode (RRDE). These results indicate that the ORR occurred

mainly via a four-electron mechanism.

Figure 6a shows the Tafel plots for the ORR on the Co-N_4-MC and Pt/C electrodes. The Co-N_4-MC electrode has a similar Tafel plot to the Pt/C electrode, indicating that the Co-N_4-MC sample has comparable kinetic performance to the Pt/C catalyst. Durability is a major issue in fuel-cell technology. Therefore, the stability of the Co-N_4-MC electrode was evaluated further. As shown in Figure 6b, no obvious change in the performance of the Co-N_4-MC electrode was observed before and after 1000 cycles. The good stability of the Co-N_4-MC electrode was attributed to the mesoporous carbon structure, which enhanced their interfacial contact and facilitated the transport of electrolyte ions (47). The unique features of the Co-N_4-MC sample, such as the graphitic mesopore framework with moderate nitrogen content, resulted in high electrocatalytic activity and excellent long-term stability.

4. Conclusion

In summary, a high-performance Co-N_4-MC electrocatalyst was prepared for the ORR. A cobalt-azide compound was used as the Co-N_4-containing precursor. An ordered mesoporous silica SBA-15 was used as a template to achieve the mesoporous structure of the Co-N_4-MC sample. The Co-N_4-MC electrode exhibited good ORR performance (similar to that of the Pt/C electrode) with good stability, which was attributed to the synergetic effects of N_4, Co and MC. Moreover, the ORR by the Co-N_4-MC sample occurred through the preferred four-electron reaction pathway. This study suggests that the Co-N_4-MC sample can be used as a non-precious electrocatalyst

for the ORR in alkaline fuel cells.

Acknowledgements

This work was supported by the Science and Technology Development Fund from Macau SAR (FDCT-098/2015/A3), the Start-up Research Grant (SRG2015-00057-FST) from Research & Development Office at University of Macau, and the UEA funding.

Appendix A. Supplementary data

Supplementary data associated with this article can be found in the online version.

References

1. L. Wang, J. Yin, L. Zhao, C. Tian, P. Yu, J. Wang and H. Fu, *Chemical Communications*, **49**, 3022 (2013).
2. H. Meng and P. K. Shen, *Electrochemistry Communications*, **8**, 588 (2006).
3. S. Zhang, Y. Shao, G. Yin and Y. Lin, *Journal of Materials Chemistry A*, **1**, 4631 (2013).
4. Y. Li, L. Tang and J. Li, *Electrochemistry Communications*, **11**, 846 (2009).
5. H. Zhao and T. Zhao, *Journal of Materials Chemistry A*, **1**, 183 (2013).
6. S. Zhang, Y. Shao, Y. Gao, G. Chen, Y. Lin and G. Yin, *Journal of Power Sources*, **196**, 9955 (2011).
7. R. Jasinski, (1964).
8. C. Mocchi and S. Trasatti, *Journal of Molecular Catalysis A: Chemical*, **204**, 713 (2003).
9. X.-Y. Xie, Z.-F. Ma, X. Wu, Q.-Z. Ren, X. Yuan, Q.-Z. Jiang and L. Hu, *Electrochimica Acta*, **52**, 2091 (2007).
10. W. Jingjie, T. Haolin, P. Mu, W. Zhaohui and M. Wentao, *Electrochimica acta*, **54**, 1473 (2009).
11. P. Convert, C. Coutanceau, P. Crouigneau, F. Gloaguen and C. Lamy, *Journal of applied electrochemistry*, **31**, 945 (2001).
12. Y. Tang, B. L. Allen, D. R. Kauffman and A. Star, *Journal of the American Chemical Society*, **131**, 13200 (2009).
13. U. I. Koslowski, I. Abs-Wurmbach, S. Fiechter and P. Bogdanoff, *The Journal of Physical Chemistry C*, **112**, 15356 (2008).
14. J. M. Ziegelbauer, T. S. Olson, S. Pylypenko, F. Alamgir, C. Jaye, P. Atanassov and S. Mukerjee, *The Journal of Physical Chemistry C*, **112**, 8839 (2008).
15. Y. Wang, Y. Nie, W. Ding, S. Chen, K. Xiong, X. Qi, Y. Zhang, J. Wang and Z. Wei, *Chemical Communications*, **51**, 8942 (2015).
16. J. Han, Y. J. Sa, Y. Shim, M. Choi, N. Park, S. H. Joo and S. Park, *Angewandte Chemie International Edition*, **54**, 12622 (2015).
17. J. Qi, L. Jiang, Q. Tang, S. Zhu, S. Wang, B. Yi and G. Sun, *Carbon*, **50**, 2824 (2012).
18. S.-H. Liu and H.-R. Syu, *Applied Energy*, **100**, 148 (2012).
19. A.-Y. Lo, C.-T. Hung, N. Yu, C.-T. Kuo and S.-B. Liu, *Applied Energy*, **100**, 66 (2012).
20. Y. Zheng, Y. Jiao, J. Chen, J. Liu, J. Liang, A. Du, W. Zhang, Z. Zhu, S. C. Smith and M. Jaroniec, *Journal of the American Chemical Society*, **133**, 20116 (2011).
21. J. Liang, Y. Zheng, J. Chen, J. Liu, D. Hulicova‐Jurcakova, M. Jaroniec and S. Z. Qiao, *Angewandte Chemie International Edition*, **51**, 3892 (2012).
22. M. B. Vazquez-Santos, E. Geissler, K. László, J.-N. Rouzaud, A. Martínez-Alonso and J. M. Tascón, *Carbon*, **50**, 2929 (2012).
23. Y. Wang, S. Tan, D. Jiang and X. Zhang, *Carbon*, **41**, 2065 (2003).
24. S.-T. Chang, C.-H. Wang, H.-Y. Du, H.-C. Hsu, C.-M. Kang, C.-C. Chen, J. C. Wu, S.-C. Yen, W.-F. Huang and L.-C. Chen, *Energy & Environmental Science*, **5**, 5305 (2012).
25. J.-H. Martens, H. Barg, M. Warren and D. Jahn, *Applied Microbiology and Biotechnology*, **58**, 275 (2002).
26. I. Herrmann, U. Kramm, S. Fiechter and P. Bogdanoff, *Electrochimica Acta*, **54**, 4275 (2009).
27. H. Liu, C. Song, Y. Tang, J. Zhang and J. Zhang, *Electrochimica Acta*, **52**, 4532 (2007).
28. M. Li, X. Bo, Y. Zhang, C. Han, N. Anaclet and L. Guo, *Journal of Materials Chemistry A* (2014).
29. S. Kattel and G. Wang, *J. Mater. Chem. A*, **1**, 10790 (2013).

30. K. N. Wood, R. O'Hayre and S. Pylypenko, *Energy & Environmental Science*, **7**, 1212 (2014).
31. X. Ge, A. Sumboja, D. Wuu, T. An, B. Li, F. T. Goh, T. A. Hor, Y. Zong and Z. Liu, *ACS Catalysis*, **5**, 4643 (2015).
32. G. Arena, A. Contino, E. Longo, D. Sciotto, C. Sgarlata and G. Spoto, *Tetrahedron letters*, **44**, 5415 (2003).
33. M. Jaroniec, J. Choma, J. Gorka and A. Zawislak, *Chemistry of Materials*, **20**, 1069 (2007).
34. J. Xu, K. Hua, G. Sun, C. Wang, X. Lv and Y. Wang, *Electrochemistry communications*, **8**, 982 (2006).
35. K. Kailasam, J. D. Epping, A. Thomas, S. Losse and H. Junge, *Energy & Environmental Science*, **4**, 4668 (2011).
36. Y. Xia and R. Mokaya, *Advanced Materials*, **16**, 1553 (2004).
37. G. Liu, X. Li, P. Ganesan and B. N. Popov, *Applied Catalysis B: Environmental*, **93**, 156 (2009).
38. Y. Yamada, J. Kim, S. Matsuo and S. Sato, *Carbon* (2013).
39. T. Sharifi, G. Hu, X. Jia and T. Wågberg, *ACS nano*, **6**, 8904 (2012).
40. H. Zhao, K. Hui and K. Hui, *Carbon* (2014).
41. A. H. M. Videla, L. Zhang, J. Kim, J. Zeng, C. Francia, J. Zhang and S. Specchia, *Journal of applied electrochemistry*, **43**, 159 (2013).
42. T. Palaniselvam, H. B. Aiyappa and S. Kurungot, *Journal of Materials Chemistry*, **22**, 23799 (2012).
43. J. Park, Y. Nabae, T. Hayakawa and M.-a. Kakimoto, *ACS Catalysis*, **4**, 3749 (2014).
44. Y. Nabae, S. Nagata, K. Ohnishi, Y. Liu, L. Sheng, X. Wang and T. Hayakawa, *Journal of Polymer Science Part A: Polymer Chemistry*, **55**, 464 (2017).
45. W. Chen, D. Ny and S. Chen, *Journal of Power Sources*, **195**, 412 (2010).
46. Z.-S. Wu, S. Yang, Y. Sun, K. Parvez, X. Feng and K. Müllen, *Journal of the American Chemical Society*, **134**, 9082 (2012).
47. L. Wang, J. Yin, L. Zhao, C. Tian, P. Yu, J. Wang and H. Fu, *Chemical Communications*, **49**, 3022 (2013).

Figure Captions

Fig. 1. Schematic diagram of the synthesis of Co-N_4-MC.

Fig. 2. TEM images (a, b, and c) and EDS (inset of c), SEM image (d) and mapping (e, f and g) of the obtained Co-N_4-MC.

Fig. 3. Adsorption/desorption curve (a), pores diameter (b) and Raman spectrum of Co-N_4-MC (c).

Fig. 4. Wide-scan X-ray photoelectron spectra (XPS) of various Co-N_4-MC (a). The XPS spectra of C1s (b), N1s (c) and Co2p (d) of Co-N_4-MC.

Fig. 5. Linear sweep (5 mV s^{-1}) of N_4-C, Co-N_4-C, Co-N_4-MC, and Pt/C in 1.0 M KOH solution saturated with oxygen (a). Linear sweeps (5 mV s^{-1}) at different rotating speeds (b). *n* value over the entire range of potentials studied (c). *n* value was measured by RRDE (d).

Fig. 6. Tafel slops of Co-N_4-MC and Pt/C electrodes (a). Linear sweep (5 mV s^{-1}) of the Co-N_4-MC electrode before (black line) and after (red line) 1000 cycles (b).

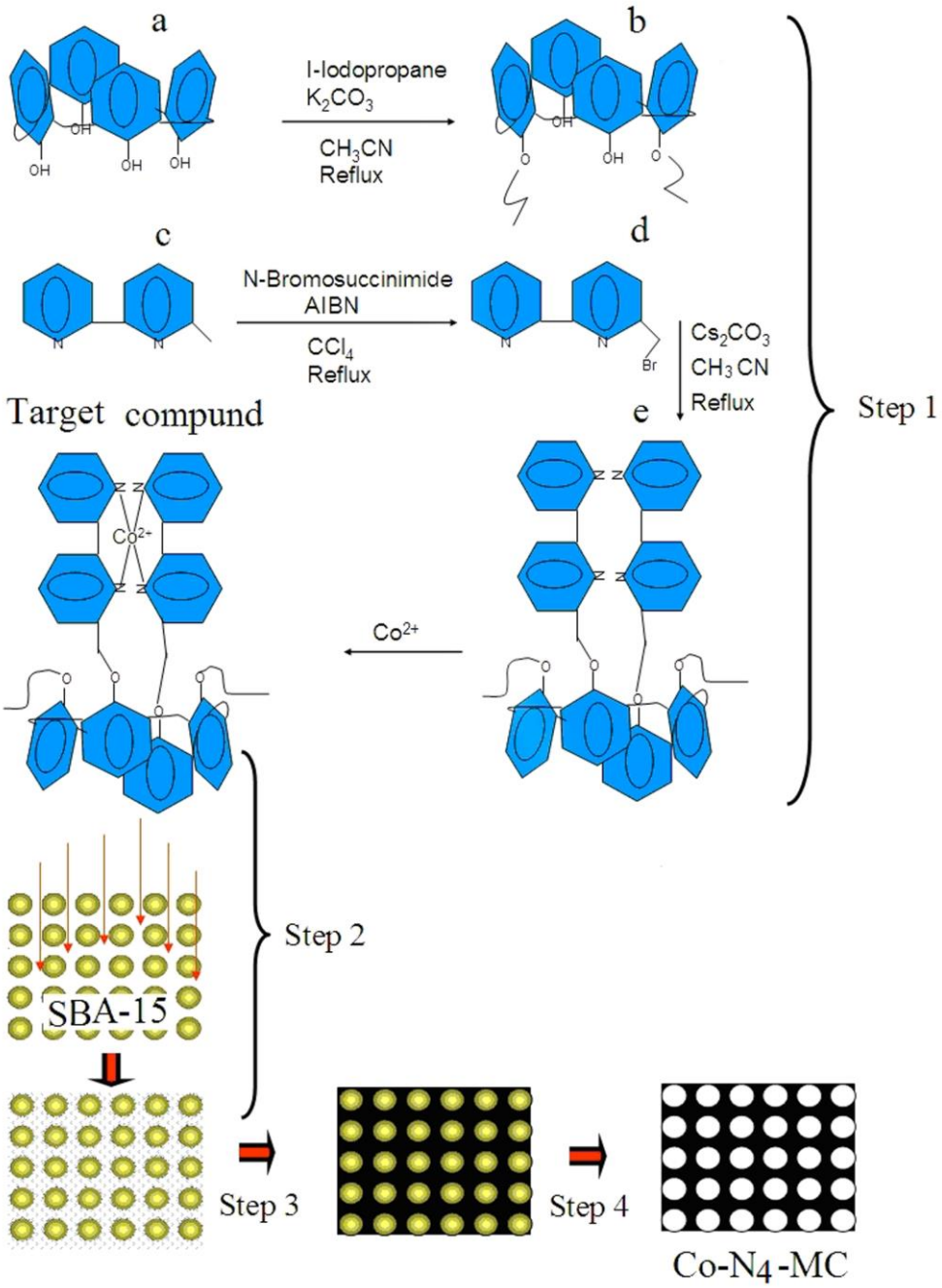

323

324 **Fig. 1.** Schematic diagram of the synthesis of Co-N_4-MC.

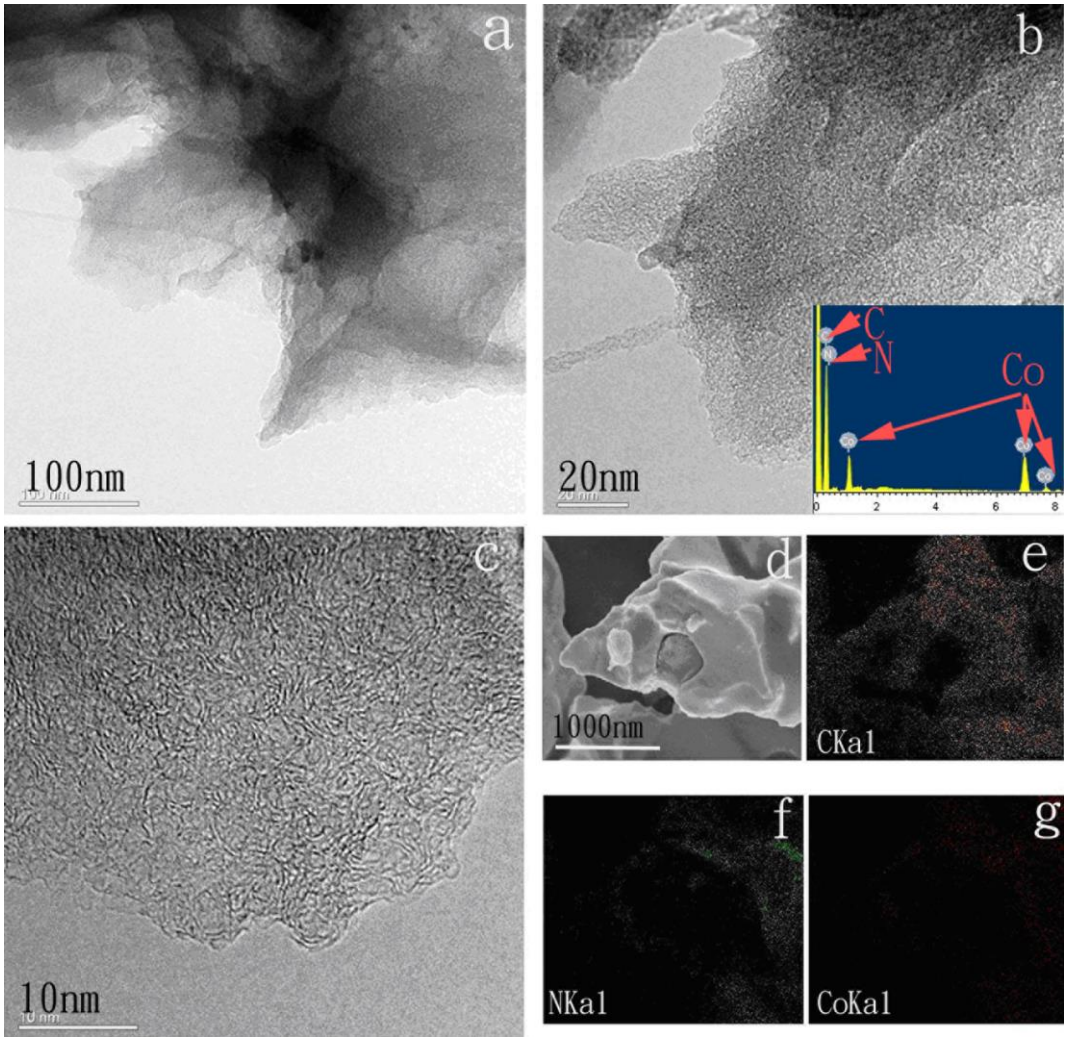

Fig. 2. TEM images (a, b, and c) and EDS (inset of c), SEM image (d) and mapping (e, f and g) of the obtained Co-N_4-MC.

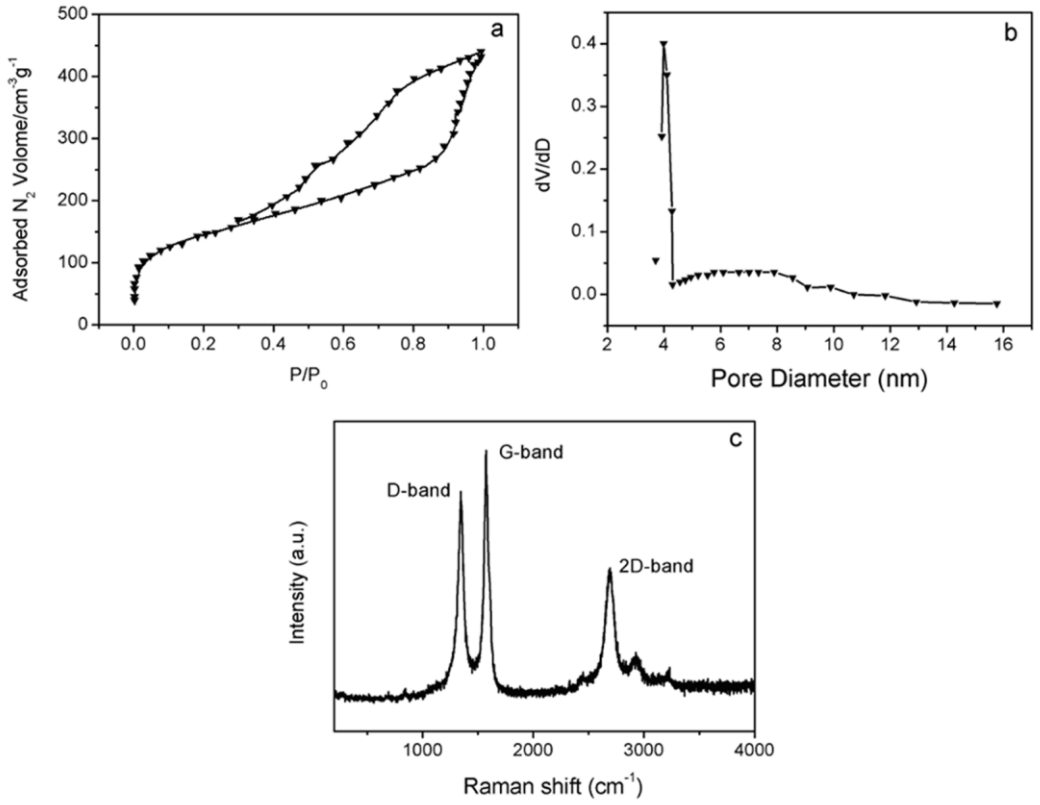

328

329 **Fig. 3.** Adsorption/desorption curve (a), pores diameter (b) and Raman spectrum of

330 Co-N_4-MC (c).

331

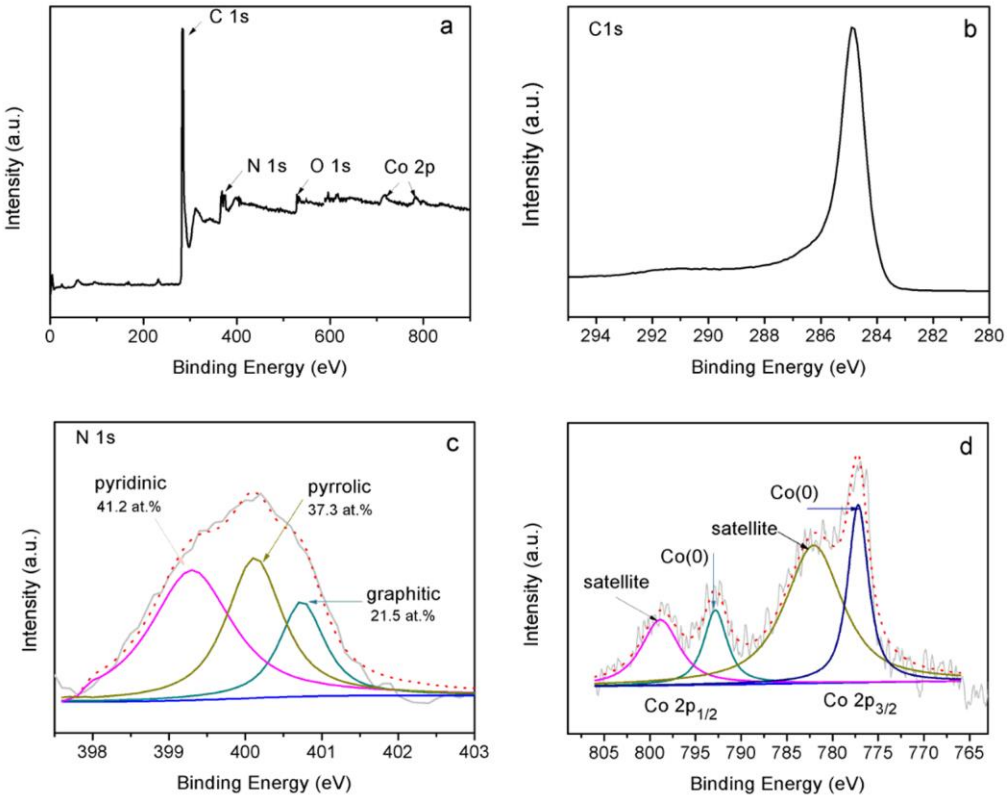

Fig. 4. Wide-scan X-ray photoelectron spectra (XPS) of various Co-N_4-MC (a). The XPS spectra of C1s (b), N1s (c) and Co2p (d) of Co-N_4-MC.

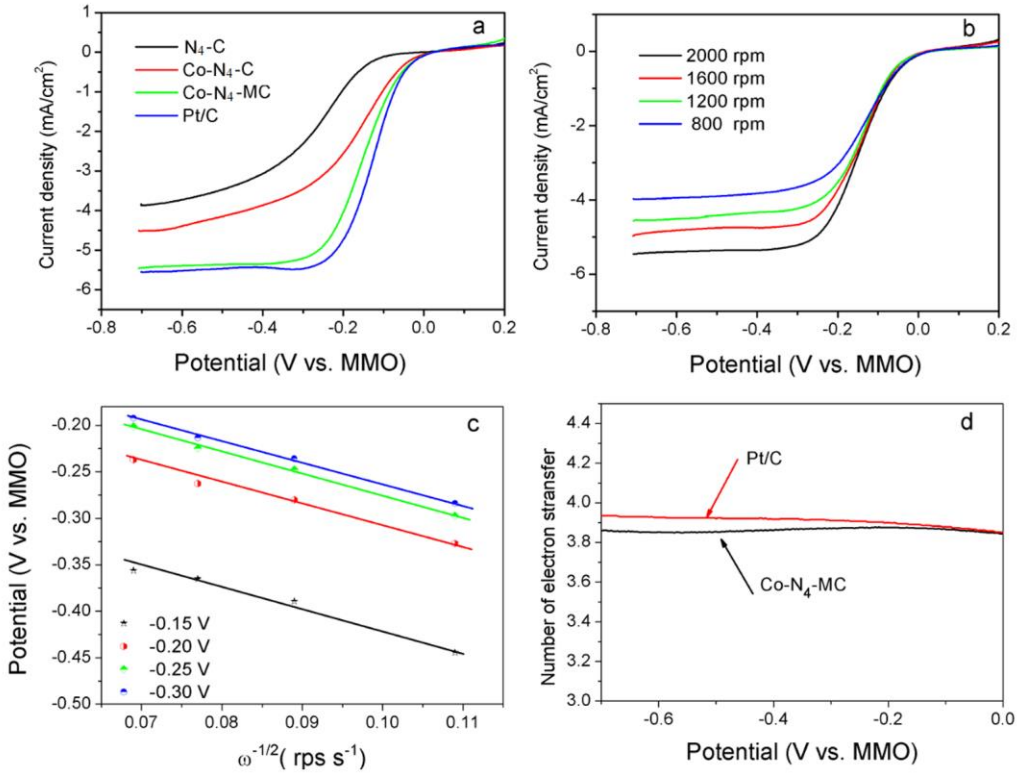

336

337 **Fig. 5.** Linear sweep (5 mV s^{-1}) of N_4-C, Co-N_4-C, Co-N_4-MC, and Pt/C in 1.0 M KOH

338 solution saturated with oxygen (a). Linear sweeps (5 mV s^{-1}) at different rotating speeds

339 (b). *n* value over the entire range of potentials studied (c). *n* value was measured by

340 RRDE (d).

341

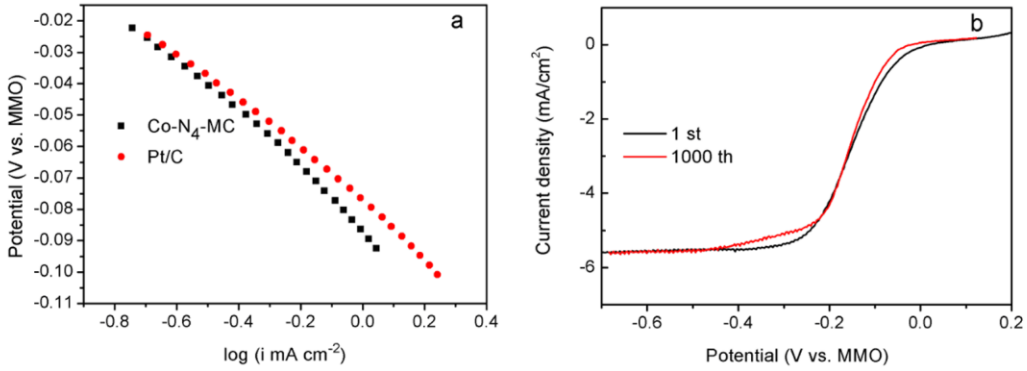

342

343 **Fig. 6.** Tafel slops of Co-N_4-MC and Pt/C electrodes (a). Linear sweep (5 mV s^{-1}) of the

344 Co-N_4-MC electrode before (black line) and after (red line) 1000 cycles (b).